AIChE

Crystal Shape Modification Through Cycles of Dissolution and Growth: Attainable Regions and Experimental Validation

Michael A. Lovette
Dept. of Chemical Engineering, University of California, Santa Barbara, CA 93106

Matteo Muratore
Dept. of Chemical Engineering, University of California, Santa Barbara, CA 93106

DIPIC-Dipartimento di Principi e Impianti di Ingegneria Chimica, Università di Padova, Via Marzolo 9, 35131 Padova PD, Italy

Michael F. Doherty
Dept. of Chemical Engineering, University of California, Santa Barbara, CA 93106

DOI 10.1002/aic.12707
Published online July 13, 2011 in Wiley Online Library (wileyonlinelibrary.com).

The impact of particle shape on end-use efficacy and downstream processing efficiency has driven industrial and academic efforts to control/manipulate the shapes obtained by crystallization. Strategies for controlling crystal shape have focused primarily on chemical routes; with shapes optimized through either solvent selection or the use of growth inhibiting additives. However, the chemical design space for crystallization may be limited, and/or the additional separation and purification steps required to remove additives or engineered solvents may be uneconomical. The application of cycles of dissolution and growth as a means for attaining desired crystal shapes is examined. A dynamic model for determining the shapes that can be attained by cycling is developed, and the results of proof of concept experiments performed using adipic acid and paracetamol are presented. The predictions obtained using the dynamic model were shown to be in good agreement with the results from the paracetamol experiments. © 2011 American Institute of Chemical Engineers *AIChE J,* 58: 1465–1474, 2012
Keywords: crystal growth, crystallization, crystal shapes, process design

Introduction

Several distinct approaches have been taken to predict and modify crystal shapes to improve end-use effectiveness[1,2] and downstream processing efficiency.[3] The term ''modified crystal shape'' refers to shapes that would not be obtained by the typical operation of a crystallization process; that is, shapes that are not obtained using the conventional solvent and temperature trajectories for the specific system, or without introducing growth inhibitors. As noted by Yang et al., the majority of these approaches have been based on solvent selection or the introduction of additives.[4,5] These methods have an intrinsic disadvantage over nonchemical routes as they may require additional separation steps to ensure the purity of the final product or for solvent recovery. Moreover, particularly within the pharmaceuticals industry, product registration may further prohibit the introduction of additional chemicals or alternative solvents.

Snyder et al.[6] and Yang et al.[5] have proposed different nonchemical routes to modify crystal shapes. Yang et al.[5] obtained modified shapes for *KDP* crystals grown in a batch cooling crystallizer, by exploiting the influence of supersaturation on the relative growth rates of different faces and accordingly using varied temperature trajectories. Snyder et al.[6] proposed the use of consecutive cycles of dissolution and growth as a means for crystal shape modification and further demonstrated the ability for crystals to acquire shapes otherwise unobtainable through single stages of either process alone. Their method exploits the differences between the crystal shape trajectories followed during growth and dissolution at the supersaturation and undersaturation used in each stage of a cycle.

The following traits have been established in the evolution of single crystal shapes: (1) as growth progresses, the shapes of a crystal with constant normal growth rates for each facet will trend toward a unique and stable steady-state growth shape regardless of its initial shape[7–9]; (2) the shapes of a crystal that is dissolving in a manner such that the dissolution rates of each face are constant, will trend away from a unique and unstable steady-state dissolution shape,[10] and (3) consecutive cycles of dissolution and growth allow for shapes that are otherwise unattainable through growth or dissolution alone for a given system.[6] In particular, the final shape of a crystal formed by alternating cycles of dissolution and growth is different from that of the same crystal grown under constant conditions.

In this article, we expand on the model developed by Snyder et al.[6] for single crystal dynamics by presenting the

Additional Supporting Information may be found in the online version of this article.

M.A.L. and M.M. contributed equally to this work.

Correspondence concerning this article should be addressed to M. F. Doherty at mfd@engineering.ucsb.edu.

global phase behaviors for growth, dissolution, and cycling processes. In doing so, we establish the regions of shapes that can be attained through growth, dissolution, or cycling, and those which cannot. Although single crystal models and experiments alone cannot account for growth rate dispersion, agglomeration or other phenomena specific to populations, they form the basis for understanding, interpreting, and predicting shape dynamics. Single crystal models and face growth rates obtained from single crystal experiments can be applied in multidimensional population balance models to provide a mapping to the shape dynamics for populations of crystals.[11–13] Additionally, the results of experiments and models performed using single crystals can provide a means for comparison with predicted and measured crystal shape dynamics for populations. The degree to which individual crystals within a population will deviate from the mapping provided by single crystal models/experiments depends on several system-specific properties. These properties include: agglomeration/breakage rates, the amount of growth rate dispersion within the population, the presence of impurities, and the rates of surface integration and transport processes.

We conclude this article with a set of single-crystal proof of concept experiments performed on paracetamol and adipic acid grown in water. These experiments were conducted in a quiescent batch crystallizer. Although these experiments do not thoroughly replicate the environment experienced by a crystal growing in a stirred tank as a member of a population, this apparatus used herein provides the ability to simultaneously measure the perpendicular growth and dissolution rates for several different faces of a crystal. Making it possible to directly compare the predictions made using our model and the experimental results for the case of paracetamol.

Shape Dynamics

To predict the effects of cycling on crystal shapes, Snyder et al.[6] developed a model that tracked the shape of a single crystal during cycles of dissolution and growth. This model determines the relative perpendicular distances of each face from an origin inside the crystal which, in conjunction with the known crystallographic data, can be used to construct the corresponding shape. The model consists of a set of ordinary differential equations; the solution to which provide these distances, and a complementary set of algebraic equations used to determine the appearance or disappearance of crystal faces from or into edges and vertices. In each application of this model, an additional set of rules were used to determine the set of N faces to be considered.[6]

The change in the perpendicular distance from a central point within the crystal to face i, denoted H_i, with time, t, is given by

$$\frac{dH_i}{dt} = G_i, \quad i = 1, \ldots, N \tag{1}$$

where G_i is the growth or dissolution rate of face i. The sign of G_i depends on whether the crystal is growing or dissolving, denoted by superscripts g and d, respectively; with G_i positive for growth and negative for dissolution. This set of N independent equations can be re-formed in terms of dimensionless variables scaled to a reference face; with the perpendicular distance, and growth and dissolution rates for this face denoted H_{ref}, $G^{\text{g}}_{\text{ref}}$, and $G^{\text{d}}_{\text{ref}}$, respectively (the notation in this article differs slightly from the original publications). For each face, the dimensionless perpendicular distance, and relative growth and dissolution rates are defined by $x_i \equiv H_i/H_{\text{ref}} > 0$, $R^{\text{g}}_i \equiv G^{\text{g}}_i/G^{\text{g}}_{\text{ref}} > 0$, and $R^{\text{d}}_i \equiv G^{\text{d}}_i/G^{\text{d}}_{\text{ref}} > 0$. Defining "warped" times for growth and dissolution as $d\xi_{\text{g}} \equiv \frac{G^{\text{g}}_{\text{ref}}}{H_{\text{ref}}}\,dt$ and $d\xi_{\text{d}} \equiv -\frac{G^{\text{d}}_{\text{ref}}}{H_{\text{ref}}}dt$, the dimensionless form of Eq. 1 is given by

$$\frac{dx_i}{d\xi_{\text{g}}} = R^{\text{g}}_{\text{i}} - x_i, \quad i = 1, \ldots, N-1 \tag{2}$$

for growth and

$$\frac{dx_i}{d\xi_{\text{d}}} = x_i - R^{\text{d}}_i, \quad i = 1, \ldots, N-1 \tag{3}$$

for dissolution; where $x_N = x_{\text{ref}} \equiv 1$. These equations are integrated from a specified initial condition (namely, $x_i(0) = x_{i,0}$ for $i = 1,\ldots, N-1$) to obtain the shape at later times ξ_g or ξ_d.

Given the crystallographic information (i.e, space group and unit cell parameters) and the relative growth or dissolution rates for the set of N faces, Eqs. 2 and 3 can be used to predict the shape evolution throughout processes of growth or dissolution, respectively. Furthermore, if the relative growth and dissolution rates are constant, Eqs. 2 and 3 are sets of independent linear ordinary differential equations with solutions given by

$$x_i(\xi_g) = R^{\text{g}}_i - \left(R^{\text{g}}_i - x_{i,0}\right)\exp\left(-\xi_{\text{g}}\right), \quad i = 1, \ldots, N-1 \tag{4}$$

for growth, and

$$x_i(\xi_d) = R^{\text{d}}_i + \left(x_{i,0} - R^{\text{d}}_i\right)\exp(\xi_{\text{d}}), \quad i = 1, \ldots, N-1 \tag{5}$$

for dissolution. In this case, Eqs. 2 and 3 each contain a unique steady-state point in $N-1$ dimensions at

$$\hat{x}^{\text{g}}_i = R^{\text{g}}_i, \quad i = 1, \ldots, N-1 \tag{6}$$

and

$$\hat{x}^{\text{d}}_i = R^{\text{d}}_i, \quad i = 1, \ldots, N-1 \tag{7}$$

When the growth or dissolution mechanisms do not change for any of the faces bounding the crystal over the range of conditions investigated, the relative growth and dissolution rates typically remain constant even if the supersaturation or undersaturation vary.[3]

These steady-state points are stable and unstable stellar nodes for growth and dissolution, respectively. This property arises from the following: (1) all of the eigenvalues of the Jacobian matrix for Eq. 2 (growth) are equal to -1; (2) conversely, all eigenvalues of Eq. 3 (dissolution) are equal to $+1$, and (3) for both equations the $N-1$ eigenvectors of the respective Jacobian matrix are orthonormal. Therefore, shape trajectories will flow along vectors connecting the initial condition and the unique steady state (a straight line in $N-1$ dimensions between the two points). For growth, trajectories will flow along this vector from the initial state toward the stable steady-state shape, which is equivalent to the Frank-Chernov shape.[7,8] After obtaining this steady state, growth will continue in such a manner that the shape is preserved.[3,9] Conversely for dissolution, shape trajectories originating at the initial state will flow along this vector in the direction away from the unstable steady state. While dissolving (at a constant undersaturation), crystal shapes will continuously

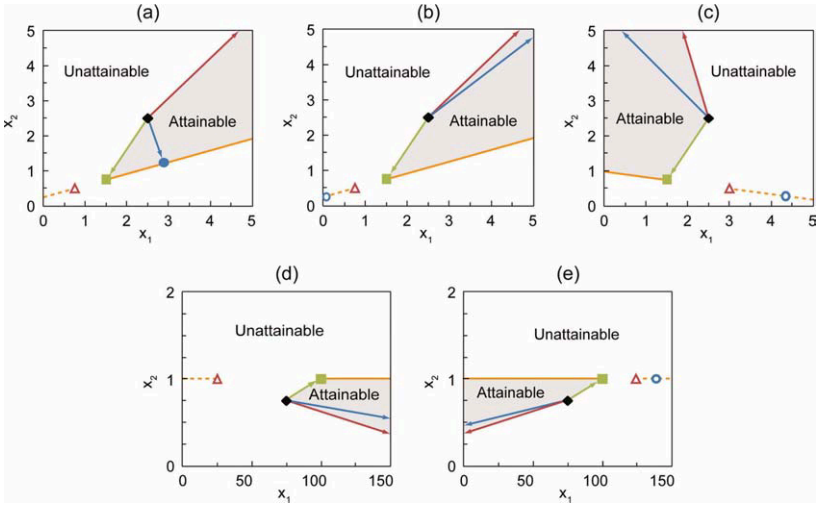

Figure 1. Representative trajectories and attainable regions in the (x_1, x_2) plane for dissolution (red), growth (green), and cycles of dissolution and growth (blue).

The black diamonds are the initial states, the blue circles are the stable (filled) and unstable (open) fixed points for cycling, and the green squares and red triangles are the steady-state growth and dissolution shapes, respectively. A typical needle-shaped crystal is considered in (d) and (e). The parameters used are listed in Table 1. [Color figure can be viewed in the online issue, which is available at wileyonlinelibrary.com.]

change until the crystal has dissolved completely. Representative trajectories for growth and dissolution are shown as green and red lines, respectively, in Figure 1. Doherty et al.,[14] have experimentally demonstrated the evolution of growing succinic acid crystals toward their stable steady-state shape, regardless of their initial condition, as well as the ability to accurately predict the shape evolution of a dissolving succinic acid crystal from its initial shape using Eq. 3.[15]

The effect of cycling on a crystal's shape can be determined by discretizing Eqs 4 and 5 to track the relative perpendicular distances of faces at the end of each cycle. In the process proposed by Snyder et al.,[6] cycles begin with a dissolution stage that lasts for Δt_d units of "real" (wall-clock) time. This time corresponds to a dimensionless warped time $\Delta\xi_d$ given by

$$\Delta\xi_d = \ln\left(\frac{H_{ref}(0)}{H_{ref}(\Delta t_d)}\right) \tag{8}$$

Dissolution stages are followed by growth stages lasting for Δt_g units of real time; corresponding to a warped time $\Delta\xi_g$ given by

$$\Delta\xi_g = \ln\left(\frac{H_{ref}(\Delta t_g)}{H_{ref}(0)}\right) \tag{9}$$

A single cycle consists of one dissolution stage followed by one growth stage. Substituting $\Delta\xi_g$ and $\Delta\xi_d$ in Eqs. 4 and 5, and using x_i ($\Delta\xi_d$) as the initial condition in each growth stage, the recursive relationship for $\boldsymbol{x}$ is given by[6]

$$\boldsymbol{x}_{j+1} = \boldsymbol{R}^g - \left(\boldsymbol{R}^g - \boldsymbol{R}^d - \left(\boldsymbol{x}_j - \boldsymbol{R}^d\right)\exp(\Delta\xi_d)\right)\exp\left(-\Delta\xi_g\right) \tag{10}$$

where $\boldsymbol{x}_j$ and $\boldsymbol{x}_{j+1}$ are the vectors of dimensionless perpendicular distances at the end of cycles j and $j+1$, respectively, and the boldface symbols define column vectors. This analysis assumes constant values of $\boldsymbol{R}^d$, $\boldsymbol{R}^g$, $\Delta\xi_d$, and $\Delta\xi_g$ for every stage of dissolution and growth, but is readily extended to the case of piecewise constant parameters that can vary between cycles. Equation 10 can be iterated from a specified initial condition (namely $\boldsymbol{x}_0$) to obtain the shape evolution as a result of performing j cycles of dissolution and growth.

Cycling Dynamics and Limiting Behavior

The recursion relation in Eqs. 10 is a set of $N-1$ independent linear difference equations, which can be written in the form

$$\boldsymbol{x}_{j+1} = \boldsymbol{a} + b\boldsymbol{x}_j \tag{11}$$

where the constant $\boldsymbol{a}$, which may be positive or negative and is potentially different for each face, is defined by

$$\boldsymbol{a} \equiv \left(1-\exp\left(-\Delta\xi_g\right)\right)\boldsymbol{R}^g - \left(\exp\left(\Delta\xi_d - \Delta\xi_g\right) - \exp\left(-\Delta\xi_g\right)\right)\boldsymbol{R}^d \tag{12}$$

and the eigenvalue b, which is the same for every face, is given by

$$b \equiv \exp\left(\Delta\xi_d - \Delta\xi_g\right) > 0 \tag{13}$$

For the case $b \neq 1$, the solution to Eq. 11 is given by

$$\boldsymbol{x}_j = b^j\boldsymbol{x}_0 + \left(\frac{1-b^j}{1-b}\right)\boldsymbol{a} \tag{14}$$

In this case, Eq. 11 has a single unique fixed-point (the discrete dynamical system equivalent of a steady state) at

$$\hat{\boldsymbol{x}}^c = \left(\frac{1}{1-b}\right)\boldsymbol{a} \tag{15}$$

or equivalently at

$$\hat{\boldsymbol{x}}^c = (1+\psi)\boldsymbol{R}^g - \psi\boldsymbol{R}^d = (1+\psi)\hat{\boldsymbol{x}}^g - \psi\hat{\boldsymbol{x}}^d \tag{16}$$

where ψ is defined by

$$\psi \equiv \frac{1-\exp(\Delta\xi_d)}{\exp(\Delta\xi_d)-\exp(\Delta\xi_g)} \tag{17}$$

The possible values of ψ are restricted to $\psi > 0$ for $\Delta\xi_g > \Delta\xi_d$ and $\psi < -1$ for $\Delta\xi_d > \Delta\xi_g$; ψ cannot lie between $[-1, 0]$. The magnitude of ψ is largest for $\Delta\xi_g \approx \Delta\xi_d$, corresponding to $b \approx 1$. Furthermore, the location of the fixed point given by Eq. 16, $\hat{\boldsymbol{x}}^c$, retains only a single degree of freedom within the $N-1$ dimensional state space and must be located along the vector containing both $\hat{\boldsymbol{x}}^g$ and $\hat{\boldsymbol{x}}^d$.

Equations 16 and 17 are the key equations that enable the prediction of the region of attainable shapes for a given set of relative growth and dissolution rates. The parameters in Eq. 16 can be separated into two distinct sets; $\boldsymbol{R}^g$ and $\boldsymbol{R}^d$ which are system-specific parameters (dependent on crystallography, solvent, supersaturation, presence of growth inhibitors) that in most cases cannot be easily manipulated, and $\Delta\xi_g$ and $\Delta\xi_d$ which are operating parameters that can be easily manipulated (by altering the times used for of the each dissolution and growth stages). The values of $\boldsymbol{R}^g$ and $\boldsymbol{R}^d$ determine the positions of $\hat{\boldsymbol{x}}^g$ and $\hat{\boldsymbol{x}}^d$, which in turn specify the direction and the location of the vector containing $\hat{\boldsymbol{x}}^c$. The values of $\Delta\xi_g$ and $\Delta\xi_d$, determine the position of $\hat{\boldsymbol{x}}^c$ along that vector as well as its stability.

We now formally state the properties of Eqs. 11–17: (1) the eigenvalues of the state matrix of Eq. 11 are all equal to b and the $N-1$ eigenvectors of the system are orthonormal, indicating that the unique fixed-point, $\hat{\boldsymbol{x}}^c$, is a stellar node; therefore (2) shape trajectories for Eq. 11 will flow in the direction of the vector connecting the initial condition and $\hat{\boldsymbol{x}}^c$; (3) $\hat{\boldsymbol{x}}^c$ will be stable for $b < 1$ and unstable for $b > 1$, corresponding to $\Delta\xi_g > \Delta\xi_d$ and $\Delta\xi_d > \Delta\xi_g$, respectively; with (4) trajectories, starting from the initial condition, moving along the vector specified by property 2 toward or away from $\hat{\boldsymbol{x}}^c$ for $0 < b < 1$ and $b > 1$, respectively; and (5) $\hat{\boldsymbol{x}}^c$ cannot be located between $\hat{\boldsymbol{x}}^g$ and $\hat{\boldsymbol{x}}^d$ because ψ cannot take values between $[-1, 0]$. These properties and their implications for attaining desired shapes by cycling are apparent in the phase planes shown in Figure 1.

As noted, $\hat{\boldsymbol{x}}^c$ is a stellar node as are $\hat{\boldsymbol{x}}^g$ and $\hat{\boldsymbol{x}}^d$ (discussed in the Introduction). Therefore, cycling trajectories will flow in the same manner as trajectories for single stages of dissolution or growth. This indicates that the differences between the shapes that can be obtained through single stages of dissolution or growth and those obtained by cycling the two processes will be determined by the differences between their respective steady states and fixed points alone.

For $b < 1$, corresponding to $\Delta\xi_g > \Delta\xi_d$, a crystal's shape will evolve toward $\hat{\boldsymbol{x}}^c$, regardless of its initial condition. However, the successive changes to $\boldsymbol{x}$ will exponentially decay with increased j due to the term b^j in Eq. 14. This decay indicates that the attainment of this fixed point may require a large (and often impractical) number of cycles. Furthermore, in cases where $a_i < 0$, the ith component of the stable fixed point, x_i, may be negative; this is a physically unattainable condition and will ultimately result in the transition of the reference face to an edge or vertex, or the disappearance of the crystal (during a dissolution stage) as cycling proceeds. This case of $a_i < 0$ as observed for paracetamol in water and is discussed in the section Paracetamol Experiments.

Criteria for the transition of facets into edges or vertices have been established by Zhang et al.[9] These criteria can be simplified if shape analyses are limited to two dimensions (i.e., convex polygons and not convex polyhedra), as was the case for the experiments in this article. Edges (the two-dimensional (2-D) analog of faces) with lengths greater than zero will be present on the bounding shape while the remaining edges will collapse into vertices. On this basis, a critical value of x_i for each edge can be established by solving for its length on the basis of the values of x describing the position of adjacent edges. For larger values of x_i the edge in question will have disappeared into a vertex. This critical value is given by

$$x_i^{\text{crit}} = \frac{1}{\sin\left(\alpha_{i-1,i}+\alpha_{i,i+1}\right)}\left(x_{i-1}\sin\left(\alpha_{i,i+1}\right)+x_{i+1}\sin\left(\alpha_{i-1,i}\right)\right) \tag{18}$$

where $\alpha_{i-1,i}$ and $\alpha_{i,i+1}$ are the interior angles between edge i and the preceding edge $(i-1)$ and the subsequent edge $(i+1)$, respectively. Similar expressions have been developed by Snyder and Doherty[16] and Szurgot and Prywer.[17]

In the limit of $b \to 0$ corresponding to $\Delta\xi_g \gg \Delta\xi_d$ and $\psi \to 0^+$, Eq. 16 gives nearly the same steady-state growth shape as Eq. 6, that is, $\hat{\boldsymbol{x}}^c \approx \hat{\boldsymbol{x}}^g$. Furthermore, for $b \to 0$, shape trajectories will follow the same path as trajectories for crystals formed by a single growth stage from the same initial conditions. This result is in agreement with intuition that when cycles are dominated by growth, the final shape and trajectory should be nearly equivalent to those attained by growing crystals in the absence of cycling. Therefore, when applied in this limit of $b \to 0$ cycling is an ineffective means for obtaining modified shapes.

The fixed point given by Eq. 15 is unstable for $b > 1$, corresponding to $\Delta\xi_d > \Delta\xi_g$ and $\psi < -1$. The eventual result of this process (with constant undersaturation) is the complete dissolution of the crystal. In this case, the trajectories will flow away from their initial states along the vector connecting the fixed point to the initial state. Representative trajectories are shown as blue lines in Figures 1b–e. In contrast to the case of $b < 1$, the changes to $\boldsymbol{x}$ will grow exponentially with j for $b > 1$. In the limit of $b \gg 1$ corresponding to $\Delta\xi_d \gg \Delta\xi_g$, Eq. 14 results in the same unstable fixed point and shape trajectory, when started from the same initial condition, that was determined for dissolving crystals in the Introduction.

For the special case $b = 1$, which corresponds to $\Delta\xi_g = \Delta\xi_d = \Delta\xi$, $\boldsymbol{a}$ will be given by

$$\boldsymbol{a} = (1-\exp(\Delta\xi))\left(\boldsymbol{R}^g - \boldsymbol{R}^d\right) \tag{19}$$

with the resulting change to $\boldsymbol{x}_j$ from its initial conditions $\boldsymbol{x}_0$, given by

$$\begin{aligned}\boldsymbol{x}_j - \boldsymbol{x}_0 &= j\,(1-\exp(-\Delta\xi))\left(\boldsymbol{R}^g - \boldsymbol{R}^d\right)\\ &= j\,(1-\exp(-\Delta\xi))\left(\boldsymbol{x}^g - \boldsymbol{x}^d\right)\end{aligned} \tag{20}$$

indicating that $\boldsymbol{x}$ will change by a constant amount after every cycle. While in this case there are no stationary states towards which or away from which crystal shapes will evolve; shape trajectories will follow paths nearly identical to those followed in the limits of b slightly greater than or slightly less than one when initiated from the same conditions.

Table 1. Parameters Used for the Trajectories Shown in Figure 1

Figure	i	$\hat{x}_{i,0}$	$\hat{x}_i^{\mathrm{g}}$	$\hat{x}_i^{\mathrm{d}}$	$\hat{x}_i^{\mathrm{c}}$	$\Delta\xi_{\mathrm{g}}$	$\Delta\xi_{\mathrm{d}}$
(a)	1	2.50	1.50	0.75	2.89	0.15	0.10
	2	2.50	0.75	0.50	1.21		
(b)	1	2.50	1.50	0.75	0.07	0.10	0.20
	2	2.50	0.75	0.50	0.27		
(c)	1	2.50	1.50	3.00	4.36	0.10	0.20
	2	2.50	0.75	0.50	0.27		
(d)	1	75.00	100.00	25.00	−19.10	0.10	0.25
	2	0.75	1.00	1.00	1.00		
(e)	1	75.00	100.00	125.00	139.70	0.10	0.25
	2	0.75	1.00	1.00	1.00		

Phase Plane Analysis

As discussed in the previous section: although, $\boldsymbol{R}^{\mathrm{g}}$ and $\boldsymbol{R}^{\mathrm{d}}$ are system-specific parameters that in most instances cannot be changed easily, $\Delta\xi_{\mathrm{g}}$ and $\Delta\xi_{\mathrm{d}}$ are readily altered by changing the time spent per cycle in each stage of dissolution and growth. Therefore, the designation of a shape region as attainable refers to the ability to attain shapes (described by $\boldsymbol{x}$) in that region by manipulating $\Delta\xi_{\mathrm{g}}$ and $\Delta\xi_{\mathrm{d}}$ for specific values of $\boldsymbol{R}^{\mathrm{g}}$ and $\boldsymbol{R}^{\mathrm{d}}$. The regions of attainable shapes dictate whether consecutive cycles of dissolution and growth (or single stages of either process) can be used to arrive at specific shapes for a given set of initial conditions and relative growth and dissolution rates. This is illustrated by the 2-D phase portraits presented in Figure 1, which were constructed for the values of $\boldsymbol{R}^{\mathrm{g}}$, $\boldsymbol{R}^{\mathrm{d}}$, $\Delta\xi_{\mathrm{g}}$, $\Delta\xi_{\mathrm{d}}$, and $\boldsymbol{x}_0$ listed in Table 1.

Changing from needle-shaped crystals that have aspect ratios $\gtrsim$100 (i.e., $x_1{:}x_2 = 1{:}\gtrsim 100$ for the cases described in Figures 1d and e) to more equant shapes that offer improved processing efficiency is of particular interest within the pharmaceuticals industry. When effective for modifying such shapes, cycling represents an ideal approach for doing so within this industry as it does not require the introduction of additional chemicals.

However, the dynamics of the cycling process require that for cycling to result in the attainment of more equant-shaped crystals, the relative dissolution rates of the slowest growing faces in the high aspect ratio direction must be larger than their relative growth rates and relative initial distances at the onset of cycling. An analogous statement can be made that for cycling to result in a lower aspect ratio, the dissolution of the crystal must result in the attainment of a lower aspect ratio shape for the given set of conditions. This requirement is illustrated by Figures 1d and e. In Figure 1d, the attainable region is limited to high aspect-ratio crystals as the unstable dissolution shape, $\hat{\boldsymbol{x}}^{\mathrm{d}}$, has a lower aspect ratio shape than the initial condition. Therefore, only similar needle-like shapes are attainable for this case by either growth, dissolution, or cycling, using any possible value of ψ. In Figure 1e, with $R_2^{\mathrm{d}} > R_2^{\mathrm{g}}$ and $R_2^{\mathrm{d}} > x_{2,0}$, the attainable region includes lower aspect ratio (non-needle like) shapes and in this or similar cases cycling can be used as a means to obtain more equant shaped crystals.

As presented, this model is limited to crystals formed as convex polyhedrons and with the growth and dissolution rates of each face independent of others (no dendrites or size dependent growth). As such, the claim that cycling may be an effective means in eliminating needle-shaped crystals only for specific conditions is asserted only within these assumptions made during the formulation of this model.

A Mathematica (version 7.0, Wolfram Inc.)[18] notebook is included in the Supporting Information that enables the construction of 2-D and 3-D phase portraits for arbitrary sets of relative growth and dissolution rates, initial conditions, and cycling times. Using this notebook, the shapes attained (in terms of the ratios of $x_1 : x_2$ or $x_1 : x_2 : x_3$) through cycling or by single stages of dissolution and growth can be determined. Using the criteria for the transition of facets into edges or vertices that have been established by Zhang et al.[9] or the 2-D analog given by Eq. 18, this notebook can be used to determine the ability to use cycling as a means for attaining crystals with specific faces present or absent from their shapes. The ability to form crystals containing specific faces is essential for broad applications including catalysis[1] and the formation of particle films to be used in plasma display panel technologies.[19]

Proof of Concept Experiments

Proof of concept experiments were carried out in a small ($\sim$4 cm^3) glass crystallizer, the contents of which were observed using an inverted optical microscope (Micromaster Inverted Digital Microscope, Fisher Scientific). This crystallizer consisted of a tapering fritted section thermally fused at its top to a threaded tube and at its base to an optical grade glass disk. The tube was threaded to allow for closure using an o-ring, a second optical grade glass disk, and a complementarily threaded cap. The optical grade glass discs at the top and bottom of the crystallizer limited the distortion of the images obtained by the microscope allowing for precise (± 5 μm) measurements to be made. The temperature within this crystallizer was controlled using a Peltier cell (HCMIS MicroIncubator, ALA Scientific Instruments). The tapered fritted section of the crystallizer was designed to ensure good thermal contact with the Peltier cell. The crystallizer and Peltier cell are shown in Figures 2a and b. This apparatus was designed to replicate a similar device developed by Vessler et al.[20]

The Peltier cell consists of two bidirectional thermoelectric elements, which transferred heat from one side (top/bottom) of the unit to the other based on the Peltier effect. The "top" side of the thermoelectric elements conductively transferred heat through the aluminum body of the Peltier cell to and from the crystallizer; while, to avoid conduction through the thermoelectric elements, the "bottom" side transferred excess heat to recirculated cooling water. The direction of heat transfer was controlled by the polarity of the current flowing to the thermoelectric elements.

The temperature of the top side Peltier cell was measured using a thermistor situated near the crystallizer. The signal from this thermistor was continuously captured by a proportional-integral (PI) controller (PTC-10, npi electronic GmbH). This controller maintained a desired set-point temperature by regulating the polarity of the current to, and the voltage difference across the thermoelectric elements. This set-point temperature and the temperature of the Peltier cell were specified and monitored by a computer which was interfaced to the controller with a USB-DAQ (USB-6281, National Instruments). The measured and set-point temperatures were obtained and specified using a LabVIEW (National Instruments) program. Optimized settings for the PI controller were determined using the Zeigler-Nichols

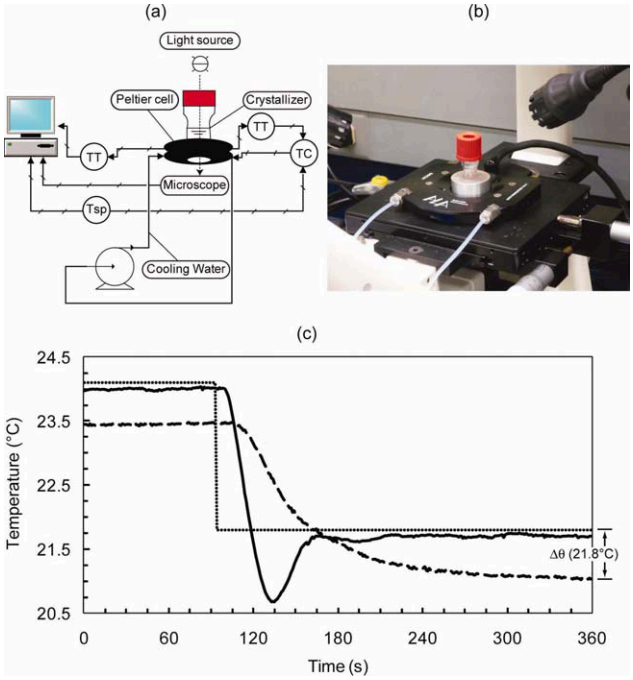

Figure 2. Experimental apparatus.

(a) Design schematic, (b) photograph of the crystallizer with cap, Peltier cell, and microscope stage, and (c) temperature response curves. In (a): TT, TC and Tsp refer to temperature transmitter, controller, and set-point, respectively, and the dotted line indicates the path of light. In (c): the dotted line is the set-point temperature (Tsp), the solid line is the temperature (TT) measured on the top side of the Peltier cell, and the dashed line is the temperature inside the crystallizer filled with ~2 cm^3 of DI water (Tcryst). [Color figure can be viewed in the online issue, which is available at wileyonlinelibrary.com.]

tuning method, with a typical post-tuning response to a 2.3°C step-change in the set-point temperature shown in Figure 1c. Calibration experiments were performed using a second thermistor placed inside the crystallizer filled with 2 cm^3 of DI water (18.2 MΩ cm) , the temperature difference $\Delta\theta$ between the solution inside the crystallizer (Tcryst, dashed line in Figure 2c) and the Peltier cell (TT, solid line in Figure 2c), was determined for 0.2°C increments over the temperature ranges investigated. For the remainder of this article, the temperatures in the crystallizer are reported as the Peltier temperature plus the offset, $T_{cryst} \approx TT + \Delta\theta$ (TT), as during experimental runs the thermistor located inside the crystallizer was not used to prevent interference with the crystallization.

The solutions used in the crystallizer were prepared in a jacketed beaker, with the necessary quantities of solute and solvent, DI water, mixed using a magnetic stir bar and held for 90 min at ~10°C above their saturation temperature. Aliquots of these solutions were transferred to the crystallizer after returning them to their saturation temperatures. The solute molecules used in these experiments were adipic acid (>99.0 wt %, Sigma-Aldrich) and paracetamol (>99.0 wt %, Sigma-Aldrich). Solubility curves for these solutions were determined using the polythermal method.[21,22]

For each experiment, seed crystals were formed through a nucleation event inside the crystallizer. The population of crystals from the nucleation event was reduced to a single crystal, when possible, by holding the temperature within the crystallizer above the solubility point for the solution. The expected result of this process was that only the largest nucleus would remain after a period of dissolution. Although this result (a single crystal) was an ideal starting point, it was not always obtained as in some instances additional crystals became apparent only after subsequent periods of growth. Due to the relatively small amount of solute incorporated by each crystal, the impacts of these additional crystals were assumed negligible. On this basis, the solution concentrations, from which the supersaturations and undersaturations are calculated, were assumed to be constant throughout each experiment, that is, $C(t) = C_0$, where $C(t)$ is the concentration of solute in the solution at time $t > 0$ and C_0 is the initial concentration.

Crystal shapes were recorded using the optical microscope throughout the dissolution and growth processes. The same 200 × magnification (a 20 × objective lens coupled with a secondary 10 × lens) was used in all experiments. Once the seed crystals reached a size on the order of 50 μm, they tended to rest in a fixed position on the bottom of the crystallizer, with care taken not to disturb this position throughout each experiment. Shape changes were quantified using Adobe Photoshop (CS3, Adobe Inc.). To determine lengths in a systematic manner, measurements were taken using the last darkened pixels occupied by the crystal along each axis.

Adipic Acid Experiments

To prepare a seed crystal of adipic acid, an aqueous solution saturated at 20.5°C, was held at 17°C inside the crystallizer. At this temperature, several nuclei formed and grew to an observable size within 1 h. The temperature was then held at 25°C until only a single crystal was visible within the crystallizer. However, on returning the solution to a supersaturated state an additional crystal was observed (upper left corner in Figures 3a and b). It was assumed that this additional crystal had only negligible effects on the shape evolution of the monitored crystal. Through subsequent periods of growth and dissolution at temperatures within ±2°C of the saturation temperature, the size and shape of the crystal observed during the cycling experiments were adjusted to the state shown in Figure 3a.

A set of 43 cycles (86 individual stages) of dissolution and growth were then performed. The temperatures used during each stage were 18 and 22°C, corresponding to bulk driving forces of $\sigma^g = 0.13$ and $\sigma^d = -0.09$; where $\sigma = \ln(C/C_{eq})$, and C_{eq} is the equilibrium concentration of solute in solution. Three cases were examined sequentially within these 43 cycles; with the crystal volume kept nearly constant, decreasing, and increasing for the first, second, and third days, respectively. The shape of the crystal changed significantly as a result of these cycles, with its evolution shown in Figure 3. A time-lapse video of the crystal throughout these cycles is included in the Supporting Information. In this video, the formation of step bunches during dissolution stages and their subsequent flow across the face during growth stages can be observed. Abu Bakar et al. observed a similar surface roughening phenomenon during thermal cycling experiments performed on sulfathiazole crystals.[23]

The lengths of crystal along axes A_1 and A_2 (labeled in Figure 3a) were measured after each stage and are shown in Figure 4a. These axes were chosen as descriptive measures of the shape because they are indicative of the chord lengths of the crystal. While the length along axis A_2 measures the

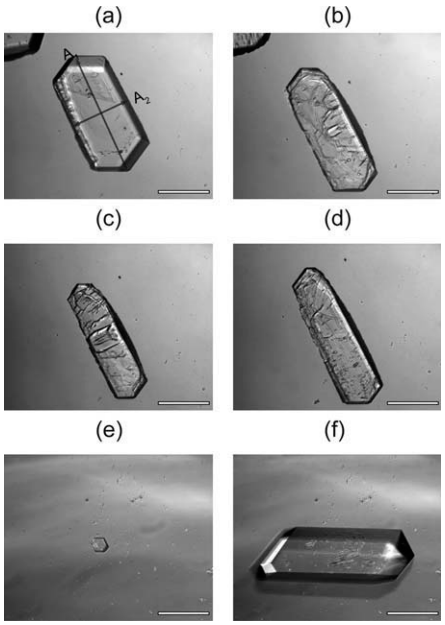

Figure 3. Adipic acid in an aqueous solution.

(a) Crystal at the beginning of the process, (b) at the end of the first day, (c) at the end of the second day, and (d) at the end of the third day. The growth and dissolution temperatures correspond to $\sigma^g = 0.13$ and $\sigma^d = -0.09$, respectively in (a)–(d). The steady-state shape for a separate control crystal, which was slowly grown (not cycled) from the seed in (e), is shown in (f). The growth temperature used in (e) and (f) corresponds to $\sigma^g = 0.04$. The scale bars correspond to 200 μm.

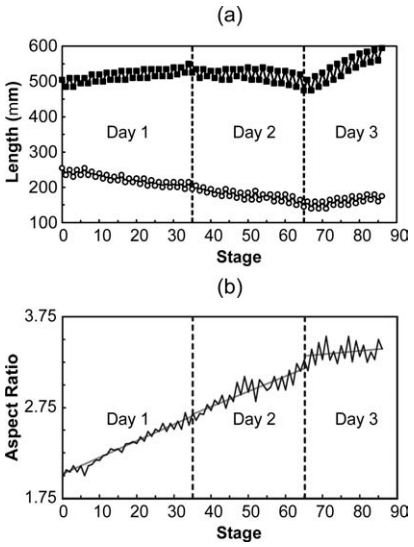

Figure 4. Shape evolution throughout the cycling experiment for adipic acid grown in an aqueous solution.

(a) The lengths along A_1 (squares) and A_2 (circles); (b) the aspect ratio (A_1/A_2) of the crystal after each stage. The straight lines in (b) correspond to the best-fit lines for aspect ratio change per stage taken over each day.

distance between two opposing faces, the length along axis A_1 measures the distance between the two most extreme points (which are edges or vertices) on the crystal. Because A_1 is not the distance between opposing faces, the symbols L_i and $\Delta L_i/\Delta t$ were used to describe the length along a given axis and the growth and dissolution rates of the crystal along that axis. This was done to distinguish these measures and those discussed in Introduction and Cycling Dynamics and Limiting Behavior sections. The aspect ratio of the crystal, taken as A_1/A_2, was used to quantify the shape change throughout the experiment and is shown after each stage in Figure 4b. The aspect ratio was increased by 70% through the course of the experiment. The rate of change in the aspect ratio of the crystal, ΔAR, decreased from 0.62 ± 0.05, to 0.52 ± 0.12, to 0.13 ± 0.24 per day, for days 1, 2, and 3, respectively.

The stage times, growth and dissolution rates, and lengths measured before and after each set of cycles, are summarized in Table 2. The values found for growth and dissolution rates are in agreement with the value of $G \approx 25$ nm/s estimated by Lovette et al. for the (spiral) growth rates of faces found for this type of crystal grown in solution.[3] Furthermore, in this case, the dissolution rates were slower than the growth rates at comparable levels of undersaturation and supersaturation. By contrast, for paracetamol in water dissolution rates were notably faster than growth rates.

In an effort to demonstrate the modified shapes that can be obtained by cycling, an additional "control" experiment was conducted. In this experiment, a different seed was grown within an aqueous adipic acid solution saturated at 18.0°C. This seed was obtained by holding the temperature of the crystallizer at 14°C until a population of nuclei had formed, and then raising the temperature to 24°C until all but one of these nuclei had dissolved completely. This seed, shown in Figure 3(e), was then grown slowly over a period of 42 h, with crystallizer held at 17.0°C corresponding to $\sigma^g = 0.04$. During this period, the crystal attained its steady-

Table 2. Stage Times, Growth and Dissolution Rates, and Crystal Dimensions at the Beginning and End of Each Day of Cycles for Adipic Acid in an Aqueous Solution, Where $\Delta L_i^g/\Delta t_g$ and $\Delta L_i^d/\Delta t_d$ are the Averaged Growth and Dissolution Rates for Axis A_i with the Error Bounds Given by the Standard Deviation During the Equivalent Stages, $L_{i,0}$ and $L_{i,F}$ and are the Initial and Final Lengths Along Axis A_i, and Δ is the Percent Change Between the Initial and Final Lengths (Corresponding to Figure 3)

Day	Δt_g (min)	Δt_d (min)	Stages (#)	Axis	$\Delta L_i^g/\Delta t_g$ (nm/s)	$\Delta L_i^d/\Delta t_d$ (nm/s)	$L_{i,0}$ (μm)	$L_{i,F}$ (μm)	Δ (%)	ΔAR (day^{-1})
1	25	60	35	A_1	14.6 ± 3.0	-5.6 ± 0.9	505	550	9	0.62
				A_2	9.0 ± 2.6	-4.6 ± 0.9	255	215	−16	
2	30	60	30	A_1	15.6 ± 4.4	-8.7 ± 2.4	525	475	−10	0.52
				A_2	8.7 ± 2.7	-5.3 ± 1.2	195	145	−21	
3	50	50	21	A_1	13.6 ± 1.6	-10.3 ± 0.7	505	595	18	0.13
				A_2	6.8 ± 1.2	-6.2 ± 0.8	160	175	9	
		Overall		A_1	14.7 ± 3.0	-7.5 ± 1.4	505	595	18	0.55
				A_2	8.1 ± 2.1	-5.0 ± 1.0	255	175	−31	

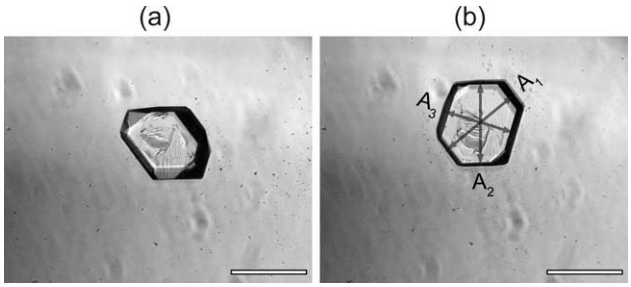

Figure 5. Paracetamol crystal in an aqueous solution (a) before and (b) after 12 cycles with 75 min of growth and 25 min of dissolution in each cycle.

The growth and dissolution temperatures correspond to $\sigma^g = 0.11$ and $\sigma^d = -0.08$, respectively. The scale bars correspond to 200 μm.

state growth shape, with growth proceeding in a shape preserving manner (this was tested by growing the crystal for another 30 hours). For comparison, this crystal is shown in its final state in Figure 3(f). The final shape of this crystal is notably different than the shapes of the cycled crystal in Figures 3(a)–(d). A time-lapse video of the growth of this control crystal is included in the Supporting Information.

Paracetamol Experiments

An aliquot from an aqueous solution of paracetamol, saturated at 22°C, was transferred to the crystallizer and held at 18°C for several hours to induce nucleation. Following the nucleation event, the solution was held above its saturation temperature until only a single crystal remained. The size and shape of this crystal were adjusted through subsequent stages of growth and dissolution at temperatures within ±2°C of the saturation temperature. Once a single seed crystal of sufficient size was obtained (shown in Figure 5), 12 cycles of dissolution and growth were performed for a period lasting 18 h.

During these cycles, the growth and dissolution times were 75 and 25 min, respectively; with the temperature of the crystallizer oscillated between 18.4 and 25°C. The growth and dissolution temperatures corresponded to $\sigma^g = 0.11$ and $\sigma^d = -0.08$, respectively. The resulting shape evolution is shown in Figure 5. A time-lapse video of the crystal throughout the experiment is included in the Supporting Information. The biased (not exclusively random) motion of small (~1 μm) material found in the crystallizer toward during growth stages and away from during dissolution stages the seed crystal is observed in the video.

The lengths of crystal along axes A_1, A_2, and A_3 at the end of each cycle, are shown in Figure 6a; with the axes labeled in Figure 5b. To analyze the shape change in accordance with the Phase Plane Analysis section, the faces perpendicular to axis A_1 were chosen as reference faces, with half the length of the crystal along this axis set as the central point.

On this basis, the warped dissolution and growth times were determined as $\Delta\xi_d = 0.14 \pm 0.02$, and $\Delta\xi_g = 0.17 \pm 0.02$ using Eqs. 8 and 9. Using Eqs. 12 and 13, the average values of the constants a_2 and a_3, and the eigenvalue b were determined as $a_2 = -0.014$, $a_3 = 0.022$, and $b = 0.97$. Therefore, given the reference face A_1, trajectories will flow toward the stable fixed point at $\hat{\boldsymbol{x}}^c$. The locations of the different fixed points in the 2-D phase plane (x_3, x_2) for this case and the corresponding predicted and observed trajectories are shown in Figure 6b. Trajectories and fixed points were predicted on the basis of the average measured growth and dissolution rates listed in Table 3.

In Figure 6b, the green square and open red triangle correspond to the growth and dissolution steady-state shapes in this plane, respectively; with the blue circle corresponding to the predicted fixed-point shape for cycling. This stationary shape (with reference faces perpendicular to A_1) is unobtainable as $x_3 < 0$. Furthermore, the disappearance of faces perpendicular to A_1 (transition to edges or vertices) is predicted

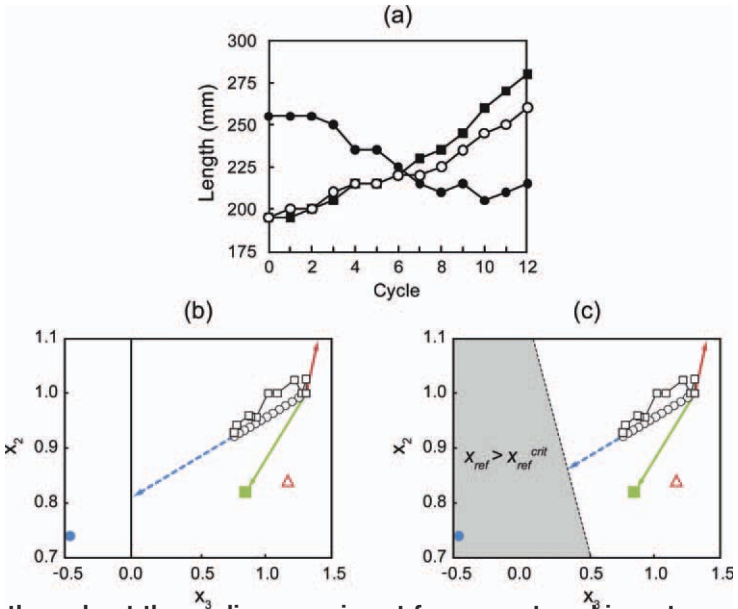

Figure 6. Shape evolution throughout the cycling experiment for paracetamol in water.

In (a): the lengths for a seed crystal of paracetamol are plotted after each cycle, with filled squares, open circles, and filled circles corresponding to the lengths measured along axes A_1, A_2 and A_3, respectively. In (b) and (c): phase planes for (x_3,x_2) are shown, with features labeled in the text. [Color figure can be viewed in the online issue, which is available at wileyonlinelibrary.com.]

Table 3. Stage Times, Growth and Dissolution Rates, and Crystal Dimensions at the Beginning and End of Each Set of Cycles for Paracetamol Grown in an Aqueous Solution (Corresponding to Figure 5)

Axis	G_i^g (nm/s)	G_i^d (nm/s)	R_i^g	R_i^d	$L_{i,0}$ (μm)	$L_{i,12}$ (μm)	$x_{i,0}$	$x_{i,12}$	$\hat{x}_i^c$
A_1	8.0 ± 1.3	−19.2 ± 2.5	1.00 ± 0.16	1.00 ± 0.13	195	280	1.00	1.00	1.00
A_2	6.4 ± 1.3	−15.6 ± 2.2	0.80 ± 0.10	0.82 ± 0.12	195	260	1.00	0.88	0.74
A_3	6.6 ± 1.4	−21.9 ± 3.3	0.86 ± 0.26	1.17 ± 0.26	255	215	1.31	0.77	−0.46

to occur for any positions in the phase plane within the greyed area of Figure 6c, which was determined by applying Eq. 18 with angles measured from Figure 5b. Thereby indicating that for states within this greyed area, A_1 is no longer an appropriate reference face. The squares and circles indicate the observed and predicted trajectories, respectively, for 12 stages; with the dashed line continuing the prediction beyond 12 stages. The agreement between the predicted and observed shape trajectories supports the analysis in the Cycling Dynamics and Limiting Behavior section.

The growth and dissolution rates, and the initial and final lengths along axes A_1, A_2, and A_3 are summarized in Table 3. The growth and dissolution rates are in qualitative agreement with the values previously determined by Shekunov and Grant for paracetamol in water using *in situ* optical interferometry.[24] Furthermore, the dissolution rates were $\sim$2.5$\times$ faster than the growth rates at comparable levels of undersaturation and supersaturation.

Conclusions

Proof of concept experiments performed on adipic acid and paracetamol have confirmed the ability to use cycles of dissolution and growth as a means for crystal shape modification. While these experiments required long times for significant shape changes to occur, the total time required is a product of the number of cycles and the time required for each stage of dissolution and growth. Based on Eqs. 8 and 9, the time required for each stage of the cycle can be approximated by $\Delta t_{g,d} \approx \Delta\xi_{g,d}\,(H_{ref}(0)/G_{g,d})$. For the systems investigated, the ratio of the initial crystal size to the growth and dissolution rates were $\mathcal{O}$(20,000) s, indicating that each cycle (with $\Delta\xi_{g,d} \approx 0.15$) will require $\sim$1.5 h. Using the apparatus detailed in Proof of Concept Experiments section lengths were limited to $\gtrsim \mathcal{O}(50)$ μm. However, as the amount of time required for each stage will scale with the initial lengths, smaller crystals will result in shorter wall-clock times per cycle and ultimately a more industrially practical process. While the number of cycles required to attain a specific distance traveled along shape trajectories decreases exponentially as the coefficient b increases, the influence of the initial state on the ultimate shape increases with b. Therefore, although operating with $\Delta\xi_d > \Delta\xi_g$ will minimize the number of cycles required to modify the crystal shape a given amount, it may require specific initial states to attain desired final shapes. This is not a requirement for performing cycles with $\Delta\xi_g > \Delta\xi_d$, as trajectories will flow toward a steady-state shape regardless of their initial states.

The results of the paracetamol experiments support the analysis of cycling dynamics presented in the Cycling Dynamics and Limiting Behavior section. These dynamics were the basis for phase plane portraits presented in the Phase Plane Analysis section which indicate that cycling is not expected to be an effective means for obtaining more equant shaped crystals in situations where needle shaped crystals were typically formed by single stages of growth, unless system dependent conditions are met. Furthermore, we have demonstrated the ability to modify the relative surface areas of specific faces by cycling, which may have an impact on the agglomeration characteristics[25] or end-product performance[19] of crystallization products. The enhancement of end-product performance through cycling is likely to be important for catalysts, for which the activity and selectivity distinctly depend on the relative surface areas of certain active faces.[1,2]

In a similar process to the cycling procedure proposed here, Abu Bakar et al.[23,26] have used thermal cycling as a means to control crystal size distribution, and polymorphic purity for populations of solution grown sulfathiazole crystals. Although the objective of their work was not shape manipulation and shapes were not quantitatively characterized, an elongation of sulfathiazole crystals after several thermal cycles can be observed by comparing Figures 5b and 12b from Ref 16. In contrast, the analysis contained in this article was limited to the evolution of shape for a single crystal. The extension of our single-crystal models to populations of crystals and further experiments determining the effects of cycling on size and shape distributions, represent promising and industrially relevant areas for future research.

Acknowledgments

The authors wish to acknowledge the financial support of Eli Lilly. The Peltier cell, inverted microscope, and USB-DAQ were purchased with the financial support of Merck. The work performed by MM was additionally supported by the Education Abroad Program at the University of California. The authors acknowledge helpful discussions with Prof. Massimiliano Barolo at the Università di Padova.

Literature Cited

1. Yang HG, Sun CH, Qiao SZ, Zou J, Liu G, Smith SC, Cheng HM, Lu GQ. Anatase TiO_2 single crystals with a large percentage of reactive facets. *Nature*. 2008;453:638–641.
2. Christopher P, Linic S. Shape- and size-specific chemistry of Ag nanostructures in catalytic ethylene epoxidation. *ChemCatChem*. 2010;2:78–83.
3. Lovette MA, Browning AR, Griffin DW, Sizemore JP, Snyder RC, Doherty MF. Crystal shape engineering. *Ind Eng Chem Res*. 2008;47:9812–9833.
4. Patience DB, Rawlings JB. Particle-shape monitoring and control in crystallization processes. *AIChE J*. 2001;47:2125–2130.
5. Yang G, Kubota N, Sha Z, Louhi-Kultanen M, Wang J. Crystal shape control by manipulating supersaturation in batch cooling crystallization. *Cryst Growth Des*. 2006;6:2799–2803.
6. Snyder RC, Studener S, Doherty MF. Manipulation of crystal shape by cycles of growth and dissolution. *AIChE J*. 2007;53:1510–1517.
7. Frank FC. On the kinematic theory of crystal growth and dissolution processes. In: *Growth and Perfection of Crystals*, Doremus RH, Roberts BW, Turnbull D, editors. Wiley: New York, 1958.
8. Chernov AA. The kinetics of the growth froms of crystals. *Sov Phys Cryst*. 1963;7:728–730.
9. Zhang Y, Sizemore JP, Doherty MF. Shape evolution of 3-dimensional faceted crystals. *AIChE J*. 2006;52:1906–1915.
10. Snyder RC, Doherty MF. Faceted crystal shape evolution during dissolution or growth. *AIChE J*. 2007;53:1337–1348.

11. Gunawan R, Fusman I, Braatz RD. High resolution algorithms for multidimensional population balance equations. *AIChE J*. 2004;50: 2738–2749.
12. Ma CY, Wang XZ, Roberts KJ. Morphological population balance for modeling crystal growth in face directions. *AIChE J*. 2008;54: 209–222.
13. Chakraborty J, Singh MR, Ramkrishna D, Borchert C, Sundmacher K. Modeling of crystal morphology distributions. Towards crystals with preferred asymmetry. *Chem Eng Sci*. 2010;65:5676–5686.
14. Gadewar SB, Hofmann HM, Doherty MF. Evolution of crystal shape. *Cryst Growth Des*. 2004;4:109–112.
15. Snyder RC, Veesler S, Doherty MF. The evolution of crystal shape during dissolution: predictions and experiments. *Cryst Growth Des*. 2008;8:1100–1101.
16. Snyder RC, Doherty MF. Predicting crystal growth by spiral motion. *Proc R of Soc A*. 2009;465:1145–1171.
17. Szurgot M, Prywer J. Growth velocities and disappearance of faces of crystals. *Cryst Res Technol*. 1991;26:147–153.
18. Wolfram Research Inc. *Mathematica, Version 7.0*: Champaign, Il, Wolfram Research, Inc. 2008.
19. Fukui Y, Terauchi M, Tsujita T. Plasma display panel and manufacturing method therefor. U.S. Patent Application Number 0157673 A1, 2008.
20. Veesler S, Lafferrere L, Garcia E, Hoff C. Phase transitions in supersaturated drug solution. *Org Process Res Dev*. 2003;7:983–989.
21. Nyvlt J, Söhnel O, Matuchova M, Broul M. *The Kinetics of Industrial Crystallization*. Elsevier: Amsterdam, 1985.
22. Muratore M. Crystal shape manipulation by means of a cycling process: theory and experiments. Master's thesis, University of California at Santa Barbara, 2010.
23. Abu Bakar MR, Nagy ZK, Rielly CD. Investigation of the effect of temperature cycling on surface features of sulfathiazole crystals during seeded batch cooling crystallization. *Cryst Growth Des*. 2010;10:3892–3900.
24. Shekunov B, Grant D. In situ optical interferometric studies of the growth and dissolution behavior of paracetamol (Acetaminophen). 1. Growth Kinetics. *J Phys Chem B*. 1997;101:3973–3979.
25. Klug DL, van Mil JH. Purification of adipic acid. U.S. Patent 5,296,639, 1994.
26. Abu Bakar MR, Nagy ZK, Rielly CD. Seeded batch cooling crystallization with temperature cycling for the control of size uniformity and polymorphic purity of sulfathiazole crystals. *Org Process Res Dev*. 2009;13:1343–1356.

Manuscript received Nov. 29, 2010, and revision received May 20, 2011.